






Relativistic effects in BDS-3 high-accuracy intersatellite time synchronization

Jianhua Yang^{a, b}, Xiaogong Hu^a , Wei Zhou^e  , Sanshi Zhou^a, Chengpan Tang^a, Yezhi Song^a, Li Liu^c, Yufei Yang^c, Qiuning Tian^{a, b}, Jinhua Liu^{a, b}, Yuchen Liu^{a, b}, Nan Xing^d, Yuexin Ma^{a, b}

^a Shanghai Astronomical Observatory, Chinese Academy of Sciences, Shanghai 200030, China

^b University of Chinese Academy of Sciences, No. 19 Yuquan Road, Beijing 100049, China

^c Beijing Satellite Navigation Center, Beijing 100049, China

^d Department of Astronomy, Beijing Normal University, Beijing 100875, China

^e Beijing Institute of Tracking and Telecommunication Technology (BITTT), Beijing Road 25, Beijing 100094, Beijing, China

Received 30 September 2022, Revised 18 February 2023, Accepted 23 February 2023, Available online 2 March 2023, Version of Record 22 April 2023.

 [What do these dates mean?](#)



Show less 

 Outline |  Share  Cite

<https://doi.org/10.1016/j.asr.2023.02.036> 

[Get rights and content](#) 

Under a Creative Commons [license](#) 

open access

Abstract

The Global Navigation Satellite Systems (GNSSs) apply conventional relativistic corrections to correct apparent clock offsets. However, with the continuous improvements made to time synchronization approaches and onboard atomic clocks, this model has obviously limits the accuracy improvements of BDS-3 intersatellite time synchronization, and also limited the apparent performance of BDS-3 onboard atomic clocks. This study demonstrates that the amplitude of GNSS conventional relativistic periodic errors can reach 0.08ns for BDS-3 MEO and IGSO satellites within a day, and 0.40ns within a month. The frequency stability of the errors' signal can reach $1.33E-14$ (approximately 10000 s) and $1.78E-15$ (approximately 1 day), and the absolute influences on the predicted clock offset accuracy can reach 0.05 ns (1 h), 1.08 ns (1 day). Notably, the above signals caused by the model errors are found in the results of current high-accuracy intersatellite time synchronization based on BDS-3 intersatellite links (ISLs). After adopting a higher-accuracy relativistic correction model, the frequency instability of BDS-3 intersatellite clock offsets is obviously reduced, and the RMS of 24h fitting residual can be reduced by approximately 60% from 0.12 ns to 0.05 ns. The average 2h 95% predicted

error decreases by approximately 17% from 0.38 ns to 0.32 ns. These results indicate that this high-accuracy relativistic correction model can improve both the BDS-3 satellites' time synchronization accuracy and the BDS-3 apparent clock offset prediction capability. This study, thus contributes to time synchronization research and signal-in-space accuracy improvements for BDS-3.



Keywords

GNSS conventional relativistic correction; Time synchronization; Clock offset estimation; Intersatellite link; BDS-3

1. Introduction

Global navigation satellite systems (GNSSs) measure distances and clock offsets by comparing clocks and provide positioning and timing services by predicting and broadcasting satellite orbits and clock offsets. Broadcasting and utilizing highly accurate clock offsets are important for improving the accuracy of these services (Montenbruck et al., 2020, Yang et al., 2021a). As a result, considering that the uncertainties in clock offset predictions are highly related to the time synchronization accuracy and the performance of atomic clocks, onboard atomic clocks and time synchronization technologies have rapidly developed since GNSSs were first introduced and have been popularized worldwide.

The onboard atomic clock is the core component of a GNSS satellite (Montenbruck et al., 2017, Wang et al., 2017), and the prediction ability of the atomic clock directly determines the accuracy of the clock offset prediction. All of the satellites in the "Big 4" GNSSs (including GPS, Galileo, BDS, GLONASS), are equipped with high-performance atomic clocks onboard, including passive hydrogen masers (PHMs), Cs, and Rubidium Atomic Frequency Standards (RAFSs) (Montenbruck et al., 2020, Yang et al., 2021a, Han and Cai, 2019). Recent research shows that the frequency instability of GNSS clocks can be less than $3.0E-15$ per day (Wu et al., 2018, Yang et al., 2019, Zhou et al., 2020). The variations in their clock offsets can be accurately modeled and predicted, which has become an effective method to calibrate the accuracy of both the time synchronization and the orbit determination (Steigenberger and Montenbruck, 2016, Li et al., 2019). Therefore, the Atomic Clock Ensemble in Space (ACES) project (Cacciapuoti and Salomon, 2011, Giorgi et al., 2019), the future GNSS Kepler constellation (Glaser et al. 2020), and the "Big 4" GNSSs all plan to carry atomic clocks with higher performance.

The prerequisite for taking full advantage of onboard high-performance atomic clocks is high-accuracy time synchronization technology (Yang et al. 2021a). The most widely applicable methods for achieving time synchronization in GNSSs are orbit determination and time synchronization (ODTS) (Montenbruck et al., 2015, Steigenberger and Montenbruck, 2016, Johnston et al., 2017) and two-way satellite time and frequency transfer (TWSTFT) (Pan et al., 2018, Tang et al., 2016, Zhou et al., 2016). Because of the poor distribution of the BDS-3 ground stations, the ODTS is not suitable for BDS to estimate satellite clock offsets (Chen et al. 2020). Therefore, the satellites of BDS-3 are equipped with onboard intersatellite link (ISL), which allows BDS-3 to use the TWSTFT method to estimate the clock offsets outside of China and its surrounding areas by directly comparing two-way ISLs (Pan et al., 2018, Tang et al., 2018). Although the TWSTFT-estimated clock offsets are free of orbital errors, they directly suffer from large measurement noise. To ameliorate this issue, a new time synchronization approach with centimeter accuracy in BDS-3 is proposed. The clock offsets estimated by this approach maintain the advantages of the TWSTFT method and suffer from less measurement errors. This approach, therefore, establishes a better foundation for further research on time synchronization with higher accuracy (Yang et al., 2021b, Yang et al., 2022).

Theoretically, referring to a sufficiently stable time reference and through accurate measurements, the onboard high-performance clock signals can be effectively described and predicted by the linear or polynomial models (Proia et al., 2014, Senior and Coleman, 2017). However, it is easy to overlook that the apparent clock offsets and apparent frequency of atomic clocks vary in different reference coordinates due to relativistic effects (Kouba, 2004, Soffel and Han, 2019). Therefore, in the evaluation of modern high-accuracy time synchronization, the influence of relativity must be considered (Kopeikin et al., 2011, Zhang et al., 2014, Colmenero et al., 2021). Within a GNSS, it is not always necessary to implement a relativistic correction as long as the GNSS-calculated clock offsets are self-consistent with the clock offsets used by the GNSS users (Kouba, 2002); However, the clock offsets without considering relativistic effects will fluctuate by approximately 10ns to 100ns, and this relativity-induced fluctuation is difficult to be predicted well by polynomial models. Therefore, BDS3 incorporates the GNSS conventional relativistic correction model into satellite multi-source observation to reduce the prediction errors caused by the relativistic effects. This practice inherits the practice of other earlier GNSS (N. Ashby, 2003, Kouba, 2019). GNSS convention relativistic correction model is fundamental but is an approximation of the exact solution. In most cases, this correction is satisfied with the sub-meter accuracy service requirements with hour-level prediction. Moreover, many scholars have derived the correction with higher accuracy, which considers the Earth J2 term both effect on orbit and frequency. And this correction has been verified well in GNSS, especially in the emerging Galileo satellite (Kouba, 2021).

With the development and updates of the time synchronization approach and onboard atomic clocks, it is possible for BDS to realize hour-level clock offsets with centimeter accuracy. The effects of GNSS conventional relativistic correction errors are nonnegligible in this context. Therefore, the preliminary study of the influence of the GNSS convention correction errors on the current BDS-3 clock offsets analysis has a certain guiding significance for constructing the next generation of BDS.

We present a numerical expression for a relativistic correction with higher accuracy in time synchronization. Then, we analyze the error characteristics of GNSS conventional relativistic corrections for BDS-3 medium Earth orbit (MEO) and inclined geosynchronous orbit (IGSO) satellites. Next, we introduce a centimeter-level intersatellite time synchronization method. Afterward, we characterize the relativistic effects that cannot be described by the GNSS conventional relativistic correction model in BDS-3 high accuracy intersatellite time synchronization and quantify the improvement in the results after adopting the proposed relativistic correction.

2. Relativistic correction model in clock offsets

2.1. Numerical correction model

According to the International Earth Rotation and Reference Systems Service (Petit and Luzum 2010), in the Geocentric Celestial Reference System (GCRS) and vicinity of the Earth, the transformation of proper time τ_A and Geocentric Coordinate Time (TCG) t can be written as:

$$\frac{d\tau_A}{dt} = 1 - \frac{1}{c^2} \left[v_A^2/2 + U_E(\vec{x}_A) + \sum_{J=1}^q V_J(\vec{x}_A, \vec{x}_E) \right] \quad (1)$$

Where c is the light speed \vec{x}_E is Earth's position. clock A is located at the GCRS coordinate position \vec{x}_A and moves with the coordinate velocity \vec{v}_A , U_E is the gravitational potential of the Earth, and V_J is the gravitational potential of the other celestial body. U_E at the $\vec{x}_A(r_A, \lambda_A, \phi_A)$ can be expanded by spherical harmonic functions up to degree N, as shown in (2) (Petit and Luzum 2010):

$$U_E(r_A, \lambda_A, \phi_A) = \frac{GM_E}{r_A} + \frac{GM_E}{r_A} \sum_{n=2}^N \left(\frac{a_e}{r_A} \right)^n \sum_{m=0}^n [\bar{C}_{nm} \cos(m\lambda_A) + \bar{S}_{nm} \sin(m\lambda_A)] \bar{P}_{nm} \sin(\phi_A) \quad (2)$$

where GM_E is geocentric gravitational constant, a_e is the equatorial radius of the Earth \bar{C}_{nm} and \bar{S}_{nm} are the

spherical harmonic coefficients, and \bar{P}_{nm} denotes Legendre polynomials. The first part of (2) is the gravitational potential of a spherical Earth, and the second part of (2) describes the nonspherical gravitational potential of the Earth.

$V = \sum_{J=1}^q V_J(\vec{x}_A, \vec{x}_E)$ is the sum of the tidal generating potential V_J which can be calculated by (3) (Petit and Luzum, 2010):

$$V_J(\vec{x}_A, \vec{x}_E) = V_J(\vec{x}_A) - V_J(\vec{x}_E) - x_A^i \partial_i V_J(\vec{x}_E) \quad (3)$$

For GNSS satellites, only the influence of Newton's gravitational potential needs to be considered (Han et al. 2021), and the first term of (3) is $\frac{GM_J}{r_{JA}}$ (M_J is the mass of celestial body J, and r_{JA} is the distance between J and the satellite), which can be spherical harmonic expansion up to degree N as $\sum_{n=0}^N \frac{GM_J}{r_J^{n+1}} r_A^n P_n(\cos(\theta_{JA}))$. The latter terms are the gravitational potential of the celestial body to the geocentric. After this, V_J can be expanded as follows (Delva et al., 2018, Han and Cai, 2019):

$$V_J = \sum_{n=0}^N \frac{GM_J}{r_J^{n+1}} r_A^n P_n(\cos(\theta_{JA})) - \frac{GM_J}{r_J} - \frac{GM_J}{r_J^2} r_A \cos(\theta_{JA}) \quad (4)$$

where r_J is the distance between the center of the Earth and celestial body J and θ_{JA} is the angle between the satellite and celestial body. Among them, the periods of θ_{JA} contain the orbital period of satellite and the revolution periods of the Earth or celestial body. r_J and θ_{JA} can be calculated by the satellite ephemeris and solar system ephemeris (Folkner et al., 2008). Combining the first term of (4) with the latter terms, the simplified form of (4) can be described as:

$$V_J = \sum_{n=2}^N \frac{GM_J}{r_J^{n+1}} r_A^n P_n(\cos(\theta_{JA})) \quad (5)$$

In the solar system, the gravitational potentials of the sun and moon are the largest for the satellites near the Earth, except for the Earth (Soffel et al., 2003, Han et al., 2021). Thus, (1) can be written as:

$$\frac{d\tau_A}{dt} = 1 - \frac{1}{c^2} \left[\frac{v_A^2}{2} + \frac{GM_E}{r_A} + R + (V_S + V_M) \right] \quad (6)$$

where V_S and V_M are the tidal generating potentials of the sun and moon, R is the second part of (2), which describes the nonspherical gravitational potential of the Earth. Then, the integral form of the second-order expansion of (6) can be written as:

$$\tau_A - \tau_{A0} = t - t_0 + \Delta t_r \quad (7)$$

where Δt_r represents the additional clock offsets caused by relativistic effects and can be written as:

$$\begin{aligned} \Delta t_r &= -\frac{1}{c^2} \\ &= \int_{t_0}^t \left[\frac{v_A^2}{2} + \frac{GM_E}{r_A} + J_2 \frac{GM_E}{r_A^3} a_A^2 \left(\frac{3}{2} \cos^2 \phi_A - \frac{1}{2} \right) + \frac{GM_S}{r_S^3} r_A^2 \left(\frac{3}{2} \cos^2 \theta_{SA} - \frac{1}{2} \right) + \frac{GM_M}{r_M^3} r_A^2 \left(\frac{3}{2} \cos^2 \theta_{MA} - \frac{1}{2} \right) \right] dt \end{aligned} \quad (8)$$

The analytical expression of (8) is difficult to derive, but the numerical expression of (8) can be simply calculated by (9):

$$\begin{aligned} \Delta t_r &= -\frac{1}{c^2} \sum_{i=1}^{(t-t_0)/h} h \left(\frac{v_{A(t_0+(i+0.5)h)}^2}{2} + \frac{GM_E}{r_{A(t_0+(i+0.5)h)}} + R_{(t_0+(i+0.5)h)} + V_{S(t_0+(i+0.5)h)} + V_{M(t_0+(i+0.5)h)} \right) \end{aligned} \quad (9)$$

where h is the integration step, which is set to 60s. For MEO and IGSO satellites, relativistic corrections can be computed with accuracies exceeding 1.0E-18s/s.

2.2. Characteristic of GNSS conventional relativistic correction model errors

Because the velocity term and geocentric potential term play a leading role in (6), the effects of the last three terms of (6) are currently ignored when GNSSs consider relativistic correction (Kouba 2004). After replacing the coordinates and velocity with osculating orbital elements, the main terms of (8) can be written as:

$$\frac{1}{c^2} \left[\frac{v_A^2}{2} + \frac{GM_E}{r_A} \right] dt = \frac{1}{c^2} \left[\frac{1}{2a} \right] dt + \frac{e\sqrt{aGM_E}}{2c^2} \cos E dE \quad (10)$$

where a is the semimajor axis, e is the eccentricity, and E is the eccentric anomaly. If the orbit without perturbation, the integral form of (10) can be written as:

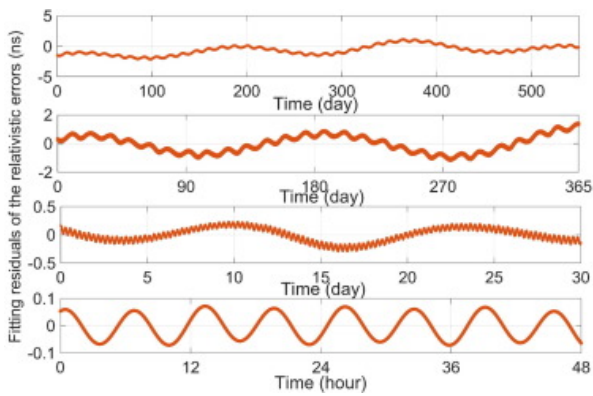
$$\begin{aligned} \int_{t_0}^t \frac{1}{c^2} \left[\frac{v_A^2}{2} + \frac{GM_E}{r_A} \right] dt &= \frac{1}{c^2} \left[\frac{1}{2a_0} \right] (t - t_0) + \frac{e\sqrt{a_0GM_E}}{2c^2} \sin E \\ &= \frac{1}{c^2} \left[\frac{1}{2a_0} \right] (t - t_0) + \frac{2\vec{x}_A \cdot \vec{v}_A}{c^2} \end{aligned} \quad (11)$$

For the BDS-3 satellite, the first term of (11) is considered to be constant and is corrected before the launch of a satellite into working orbit. The variation of the second term is caused by the eccentricity and eccentric anomaly, so the second term of (10) is called as the relativistic eccentricity correction at the earlier time (N. Ashby, 2003). For GNSSs, probably because the relativistic eccentricity correction is widely adopted by the GNSS to correct clock signals, it also is called as GNSS conventional relativistic correction (Kouba, 2002, Kouba, 2019; IERS2010). However, due to all kinds of perturbations, the variations in the orbital elements can be 1.0E-3 times the mean orbital elements (Kozai, 1959). Moreover, solar and lunar effects are not considered in GNSS conventional relativistic corrections. Contributions of the higher-order relativistic terms in the expansion of the geopotential and the Earth's tidal potential have been discussed and measured in the Galileo satellites in eccentric orbit (Delva et al., 2015, Delva et al., 2018, Hermann, et al., 2018). While previous works have already discussed and improved the relativity correction model, whether the GNSS conventional relativistic correction errors can be detected by the BDS clock offsets is still worth studying. The GNSS conventional relativistic correction error can be calculated as:

$$Er r^r = \Delta t_r - \Delta t_c \quad (12)$$

Where $\Delta t_c = \frac{2\vec{x}_A \cdot \vec{v}_A}{c^2}$ is the GNSS conventional relativistic correction, $Er r^r$ is the GNSS conventional relativistic correction error. From the (8) and orbit theory, the $\frac{3}{2} \cos^2 \theta - 1$, $\frac{3}{2} \cos^2 \theta_{MA} - 1$, $\frac{3}{2} \cos^2 \theta_{SA} - 1$ are not only explicit in the (8), they but also are implicit in \vec{r}_A . Therefore, there are at least three kinds of period terms in the high-accuracy relativistic correction, which are respectively relative to 2θ (approximately half of the orbital period), $2\theta_{MA}$ and $2\theta_{SA}$ (approximately half of the lunar revolution period at about 14days and half of the Earth's revolution cycle at about 182days). It is worth mentioning that earlier studies already derived the approximate analytical solution of relativity effects caused by the J2 term, and some studies further find it is in good agreement with Galileo satellite clock signals. (Kouba, 2021, Formichella et al., 2021).

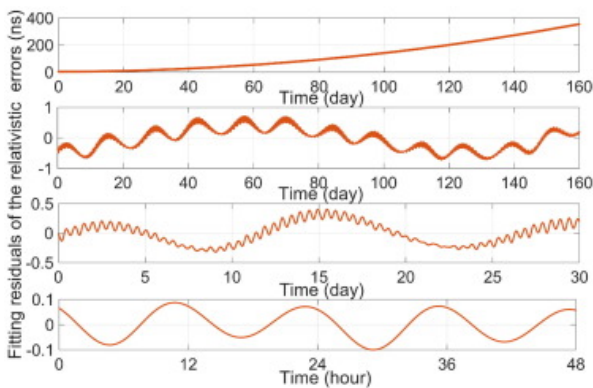
Based on the broadcast ephemeris of BDS-3 (beginning with January 1st, 2020), the sequence of GNSS conventional correction errors can be calculated by (8). The above three kinds of periodic signals of relativity correction in MEO and IGSO can be extracted by linear or quadratic fitting residuals of the error sequence, which are shown in Fig. 1 and Fig. 2 respectively. For BDS-3 MEO (C26), the amplitude of half-year, half-month, half-orbit periodic error can respectively reach 1.4, 0.3, and 0.07ns, respectively. For BDS-3 IGSO (C38), after the 160days, GNSS conventional relativistic error for IGSO platforms can reach 340ns (top panel), and the frequency drift is approximately $2.0E-21 s/s^2$. The reason for this frequency drift is suspected to be the long-period variation in the IGSO semimajor axis caused by the orbital resonance of the tesseral harmonics generated by perturbations of the Earth (Liu, 1977a, Liu, 1977b). This means that a linear polynomial is not suited to describe and predict long-term IGSO clock offsets under GNSS conventional relativistic corrections. After deducting the long-term errors, the amplitude of half-month periodic error can reach 0.40ns (third panel), and the amplitude of half-orbit periodic error can reach 0.08ns (bottom panel).



[Download : Download high-res image \(185KB\)](#)

[Download : Download full-size image](#)

Fig. 1. Fitting residuals of the GNSS conventional relativistic correction errors for a BDS-3 MEO satellite (C26). The sequences are obtained by linear fitting of the GNSS relativistic error in different time scale.

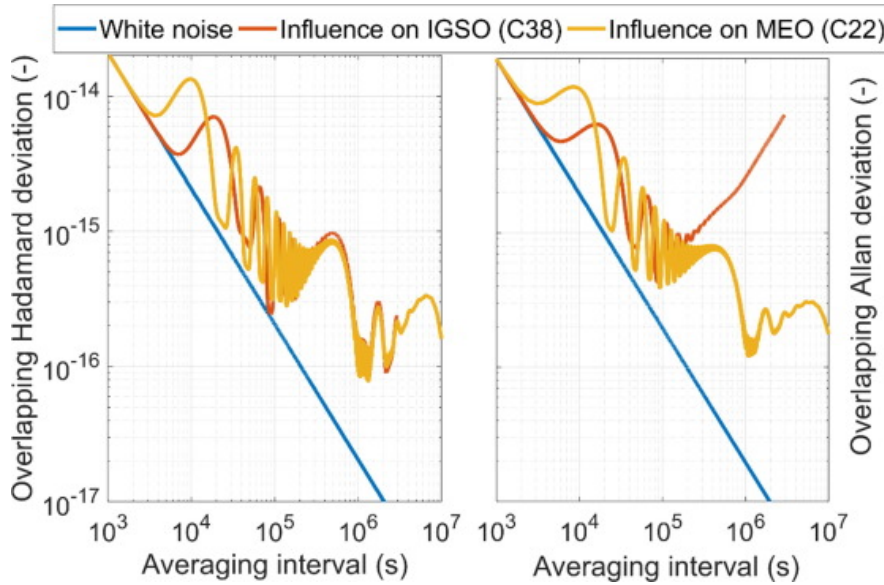


[Download : Download high-res image \(178KB\)](#)

[Download : Download full-size image](#)

Fig. 2. Fitting residuals of the GNSS conventional relativistic correction errors for a BDS-3 IGSO satellite (C38). The sequence of the top panel is obtained by linear fitting of the GNSS relativistic errors. Others are obtained by quadratic fitting model.

The blue lines in Fig. 3 represent the frequency stability of the white noise with STD of 0.01 ns. Based on the blue line, the red and orange lines represent the effects of GNSS conventional relativistic errors on the frequency stability of BDS-3 MEO and BDS-3 IGSO satellites. Fig. 3 clearly demonstrates that the frequency instability of both MEO and IGSO satellites increases gradually when the interval exceeds 10000s. The periodic signal in the GNSS conventional relativistic errors is like an approximate sinusoid. Then many bumps in the frequency stability are caused by the superposition of the approximate sinusoid signals on the white noise (Carson and Haljasmaa 2015). For MEO platforms, the effects of relativistic errors on the frequency stability can reach $1.33\text{E-}14$ at an interval of approximately 10000s and $1.78\text{E-}15$ at an interval of approximately 1 day (81000s). For IGSO platforms, the effects of relativistic errors on the Hadamard deviation can reach $6.37\text{E-}15$ at an interval of approximately 10000s and $2.15\text{E-}15$ at an interval of approximately 1 day. Notably, due to the frequency drift caused by the longer long-period terms of the errors (Liu, 1977a, Liu, 1977b), the Allan deviation of relativistic errors on IGSO satellites increases obviously at intervals higher than 10000s. The frequency instability of the bumps within a few days is greater than the frequency instability of the BDS-3 onboard clock (Shuai et al., 2021, Mei et al., 2021). It means that the GNSS conventional relativistic errors will deteriorate the evaluation of the BDS-3 onboard atomic clocks.

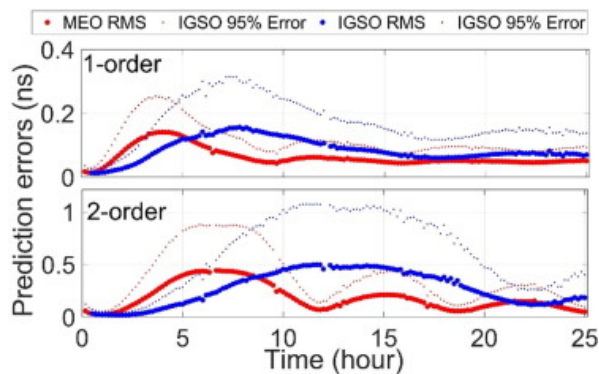


[Download : Download high-res image \(445KB\)](#)

[Download : Download full-size image](#)

Fig. 3. Frequency stability of GNSS conventional relativistic correction errors. The blue lines, yellow lines, and the red lines are the frequency stability of 0.01 ns white noise sequence and the frequency stability of the sequence with GNSS conventional relativistic correction errors for MEO and IGSO.

The GNSS conventional relativistic errors will also affect the prediction ability of clock offsets between high-performance clocks. Similarly, we introduce ϵ_{rr} in (12) on 0.01 ns white noise to analyze the theoretical influence of the GNSS relativistic conventional model error on the atomic clock prediction. Results of BDS-3 IGSO and MEO are plotted in Fig. 4. In the prediction, the predicted data are generated by the low order polynomial model and guaranteed to be of the same duration as the fitting data. Fig. 4 suggests that if a linear model (adopted by PHMs) is used for the prediction, the maximum 95% predicted error within a day can reach 0.25 ns and 0.31 ns for MEO and IGSO satellites, respectively. The influences of the 95% 1h and 2h predicted errors on BDS-3 MEO platforms can reach 0.08 ns and 0.15 ns, and the corresponding influences on BDS-3 IGSO platforms can reach 0.02 ns and 0.06 ns. If a quadratic model (adopted by RAFSs) is used for prediction, the maximum 95% predicted error over the course of a day can reach 0.25 ns and 0.31 ns for MEO and IGSO satellites. Likewise, the influences of the 95% 1h and 2h predicted errors on BDS-3 MEO platforms can reach 0.05 ns and 0.15 ns, and the corresponding influences on BDS-3 IGSO platforms (C38) can reach 0.05 ns and 0.04 ns.



[Download : Download high-res image \(189KB\)](#)

[Download : Download full-size image](#)

Fig. 4. Daily prediction ability of GNSS conventional relativistic correction errors.

3. BDS-3 high-accuracy intersatellite clock offsets estimated method

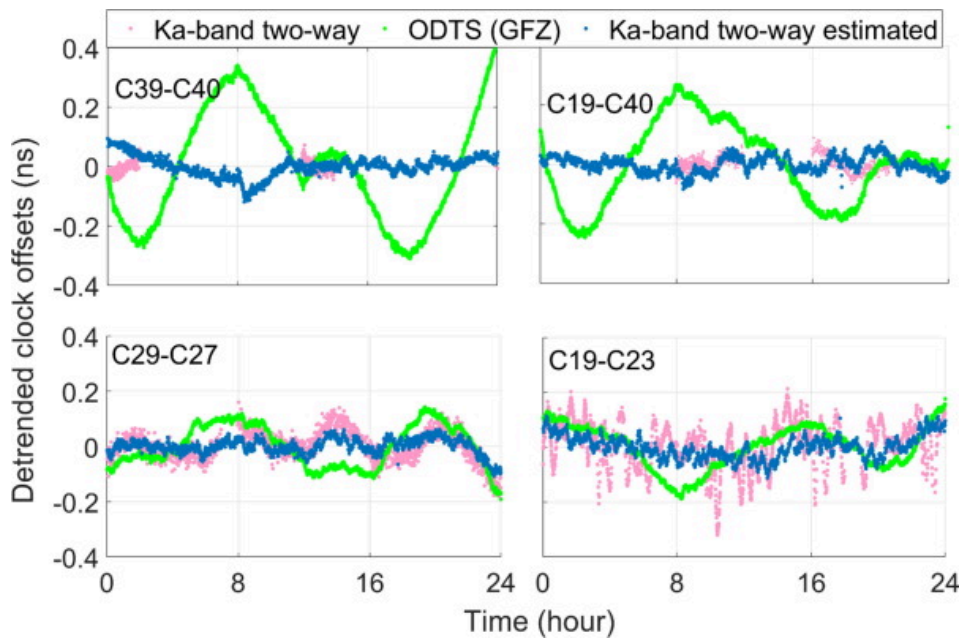
BDS-3 satellites are equipped with Ka-band facilities to circumvent the lack of globally distributed ground observation stations. Ka-band ISL facilities enable dual time-division multiple access (TDMA) one-way measurements, meaning that one satellite can establish connections with different satellites at different times within a connectivity cycle (60s). Based on the corresponding ISLs, the Ka-band two-way intersatellite clock offsets can be directly calculated as:

$$cl\ k_{BA}(t_0) = \frac{\rho_{AB}(t_0) - \rho_{BA}(t_0) - |\vec{R}_{AB} - \vec{R}_{BA}|}{2c} - \frac{\tau_A^{Send} - \tau_A^{Rcv}}{2c} + \frac{\tau_B^{Send} - \tau_B^{Rcv}}{2c} - \frac{\Delta\rho_{cor}^{AB} - \Delta\rho_{cor}^{BA}}{2c} \quad (13)$$

where t_0 is the target epoch described by TCG; $cl\ k_{BA}(t_0)$ denotes the apparent clock offsets between satellites A and B (referred to as the Ka-band two-way intersatellite apparent clock offsets in the remainder of this paper); $\rho_{BA}(t_0)$ and $\rho_{AB}(t_0)$ are the measurement values reduced from different times to the target epoch (details regarding the reduction method can be found in [Tang et al.2018](#)); \vec{R}_{AB} and \vec{R}_{BA} are the relative coordinate vectors between satellites A and B; c is the speed of light; τ_A^{Send} and τ_B^{Send} are the send delays of satellites A and B, respectively; τ_A^{Rcv} and τ_B^{Rcv} are the receive delays of satellites A and B (the time delay can be solved using the method of Pan et al.); and $\Delta\rho_{cor}^{AB}$ and $\Delta\rho_{cor}^{BA}$ are the correction errors, including phase center corrections and time bias corrections (to describe apparent clock offsets, the relativistic delay is deliberately ignored here).

Within a connectivity cycle, approximately 300 Ka-band two-way intersatellite clock offsets can be estimated by (13). While only some of these offsets are needed to achieve time synchronization between all satellites, redundant clock offsets can be valuable for further estimating the intersatellite clock offsets with higher accuracy via indirect adjustment. The intersatellite clock offsets estimated by indirect adjustment are referred to as Ka-band estimated intersatellite clock offsets or high-accuracy intersatellite apparent clock offsets in this paper. The clock offsets estimated by this approach in BDS-3 are called Ka-band two-way estimated intersatellite clock offsets.

The intersatellite clock offsets of C39-C40 (IGSO-IGSO), C39-C19 (MEO-IGSO), C29-C27 (MEO on the same orbital plane), and C19-C23 (MEO on different orbital planes) are taken as examples. After applying GNSS conventional relativistic corrections and detrending the same trend, the Ka-band two-way estimated clock offsets and ODTS precise intersatellite clock offsets provided by the German Research Centre for Geosciences (GFZ) Multi-GNSS Experiment (MGEX) are compared in [Fig. 5 \(Deng et al., 2022\)](#). Wherein the pink lines describe the direct Ka-band intersatellite clock offsets, the blue lines describe the Ka-band estimated intersatellite clock offsets, and the green lines describe the GFZ intersatellite clock offsets. Despite compared to the GFZ intersatellite clock offsets, the Ka-band intersatellite clock offsets contain larger noise levels, the Ka-band two-way intersatellite clock offsets exhibit weaker orbital fluctuations, especially for IGSO satellites. More details and advantages can refer to [Yang et al.2022](#).



[Download : Download high-res image \(393KB\)](#)

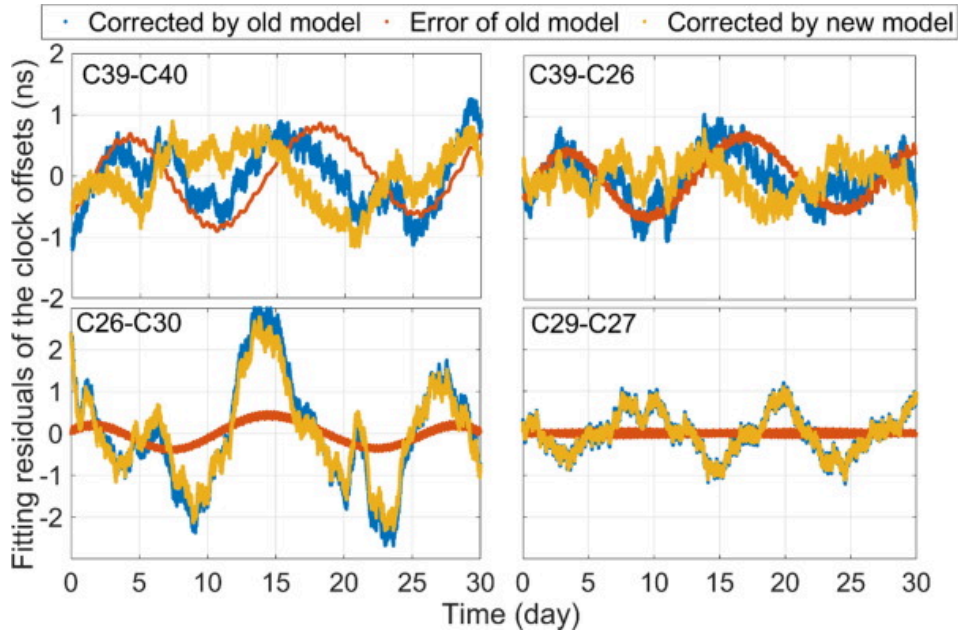
[Download : Download full-size image](#)

Fig. 5. Clock offset comparison among Ka-band two-way estimated intersatellite clock offsets, Ka-band two-way intersatellite clock offsets, and GFZ ODTs intersatellite clock offsets. All of them are only corrected by GNSS conventional relativistic correction.

While the Ka-band inter-satellite estimated clock offsets are affected by the magnetic field, temperature, and illumination of the sun. The above results indicate that the Ka-band two-way intersatellite clock offsets retain the advantages of the direct ISL comparison, being free of orbital errors and having smaller measurement errors and suffering from less noise by adjusting redundant clock offsets. This means that the Ka-band estimated intersatellite clock offsets are more accurate, at least on the 1-day timescale.

4. Effects in BDS-3 intersatellite clock offsets

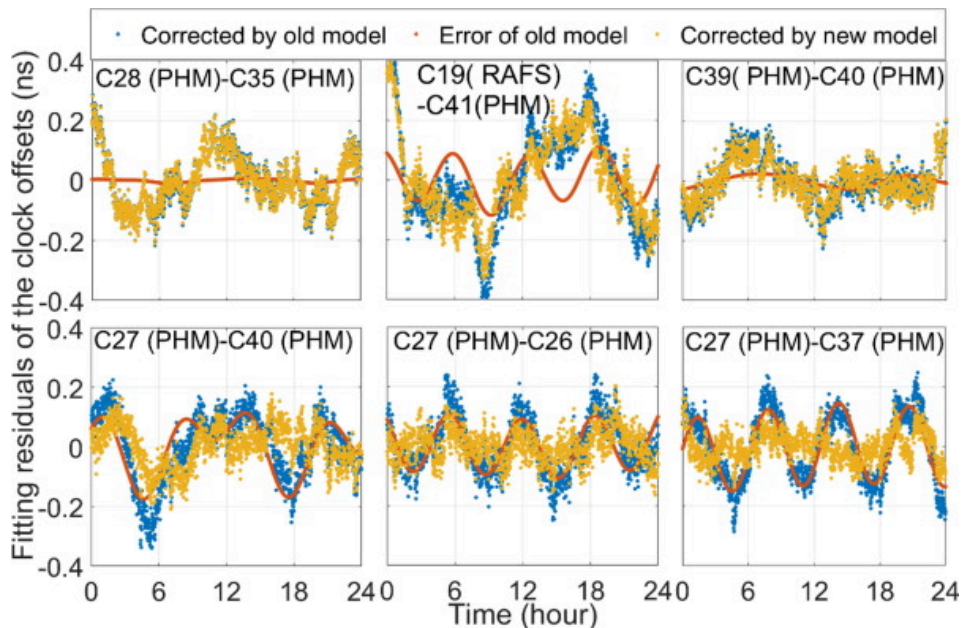
[Fig. 6](#) and [Fig. 7](#) describe the typical intersatellite fitting residuals of intersatellite clock offsets under different relativistic correction models. The blue lines are the detrended clock offsets under GNSS conventional relativistic corrections. The red lines are the detrended GNSS conventional relativistic correction errors. The yellow lines are the detrended clock offsets under the high-accuracy relativistic correction. Unless otherwise noted, the clock offsets mentioned in the following are between the PHMs ([BaoJun et al., 2021](#)).



[Download : Download high-res image \(419KB\)](#)

[Download : Download full-size image](#)

Fig. 6. Thirty-day intersatellite clock offsets under different relativistic corrections. Blue and orange curves are the clock offsets respectively corrected by GNSS conventional relativistic correction and high-accuracy relativistic correction. Red curves are the periodic errors of GNSS conventional relativistic correction.



[Download : Download high-res image \(602KB\)](#)

[Download : Download full-size image](#)

Fig. 7. Intersatellite clock offsets under different relativistic corrections. Blue and orange curves are the clock offsets respectively corrected by GNSS conventional relativistic correction and high-accuracy relativistic correction. Red curves are the periodic errors of GNSS conventional relativistic correction.

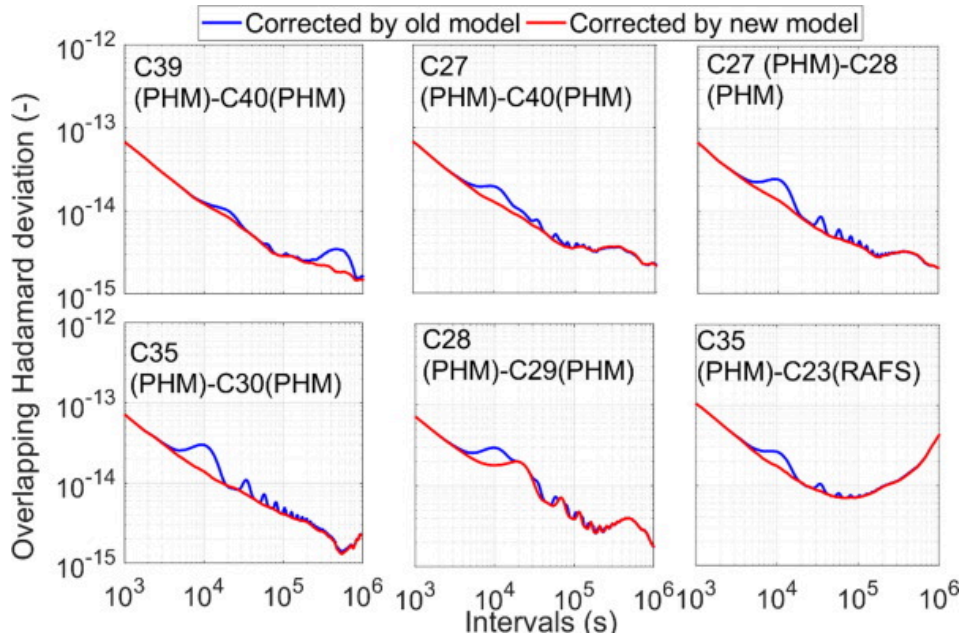
For the intersatellite clock offsets between BDS-3 satellites, the amplitude of the half-month periodic term of GNSS conventional relativistic correction errors is determined mainly by the difference between the longitudes of the ascending node (Ω) of the two satellites. The top left panel of Fig. 6 describes the 30day fitting residual of the intersatellite clock offsets between two IGSO satellites under different relativistic corrections. Corrected by the GNSS conventional relativistic model, the RMS of the 30day fitting residual is 0.49ns. Further deducting the GNSS conventional relativistic correction error reduces the RMS by approximately 10% to 0.44. top right panel of Fig. 6 describes the 30day fitting residual of clock offsets between IGSO and MEO satellites under different relativistic corrections. Corrected by the GNSS conventional relativistic model, the RMS of the residual is 0.39ns. Furthermore, deducting the GNSS conventional relativistic correction error reduces the RMS by approximately 28% to 0.28ns. Bottom left panel of Fig. 6 describes the 30day fitting residual of clock offsets between two MEO satellites on different orbital planes (different Ω) under different relativistic corrections. Corrected by the GNSS conventional relativistic model, the RMS is 1.31 ns, and further deducting the GNSS conventional relativistic correction error reduces the RMS by approximately 2.3% to 1.28ns. The bottom right panel of Fig. 6 describes the 30day fitting residual of clock offsets between two MEO satellites on the same orbital plane. When the satellites are on the same orbital plane, they have similar Ω , and thus, their half-month periodic terms cancel each other out; therefore, the half-month periodic term has little effect on the intersatellite clock offsets between two satellites on the same orbital plane.

The amplitude of the half-orbit periodic term of the GNSS relativistic correction error for a BDS-3 MEO satellite is mainly relative to the true anomalies f instead of Ω of the two satellites. The typical 24h fitting residuals of intersatellite clock offsets under different GNSS relativistic corrections are plotted in Fig. 7. The top left panel of Fig. 7 describes the fitting residuals of the clock offsets between two MEO satellites with the same $2f$ parameter, which means that the half-orbit periodic term errors cancel each other out, and thus, the $2f$ term has little effect on clock offsets. the top middle panel of Fig. 7 describes the fitting residuals of the clock offsets between RAFS and PHM on BDS-3 MEO platforms. Although the process noises of RAFSs dominate the fitting residuals, deducting the GNSS conventional relativistic correction error reduces the RMS of the residuals by approximately 16% from 0.19ns to 0.14ns. The top right panel of Fig. 7 describes the fitting residuals of the clock offsets between two IGSO satellites. After deducting the GNSS conventional relativistic correction error, the RMS of the residuals is decreased by approximately 11% from 0.073ns to 0.065ns. The bottom left panel of Fig. 7 describes the fitting residuals of the clock offsets between IGSO and MEO satellites. After deducting the GNSS conventional relativistic correction error, the RMS of the residuals decreases by approximately 39% from 0.114ns to 0.070ns. The bottom middle panel of Fig. 7 describes the fitting residuals of the clock offsets between two MEO satellites on different orbital planes. After deducting the GNSS conventional relativistic correction error, the RMS of the residuals is reduced by approximately 48% from 0.089ns to 0.055ns. Bottom right panel of Fig. 7 describes the fitting residuals of the clock offsets between two MEO satellites on the same orbital plane. Deducting the GNSS conventional relativistic correction error reduces the RMS of the residual by approximately 58% from 0.117ns to 0.050ns.

On the long-term scale, the process noises of atomic clocks dominate the fitting residuals of the intersatellite clock offsets. Therefore, from the perspective of the long-time fitting residuals, the improvements after replacing the GNSS conventional relativistic correction with a high-accuracy relativistic correction are not obvious. However, on the scale from a few hours to a few days, which represents one of the most important time scales in current GNSSs, the influence of classic relativistic errors on the fitting residual is close to 60%, indicating that the half-orbit periodic terms of GNSS conventional relativistic correction errors seriously affect the fluctuation of the fitting residuals. Therefore, if higher-accuracy time synchronization and higher-performance onboard atomic clocks are the targets, describing the clock offsets under the proposed high-accuracy relativistic frame is necessary.

Frequency stability analysis is able to reflect the advantages of the high-accuracy relativistic correction model. Fig. 8 plots the representative overlapping Hadamard deviations of intersatellite clock offsets under different relativistic corrections. The blue lines are the Hadamard deviations of intersatellite clock offsets under the GNSS conventional

relativistic correction, whereas the red lines are the Hadamard deviations of intersatellite clock offsets under the high-accuracy relativistic correction.



[Download : Download high-res image \(563KB\)](#)

[Download : Download full-size image](#)

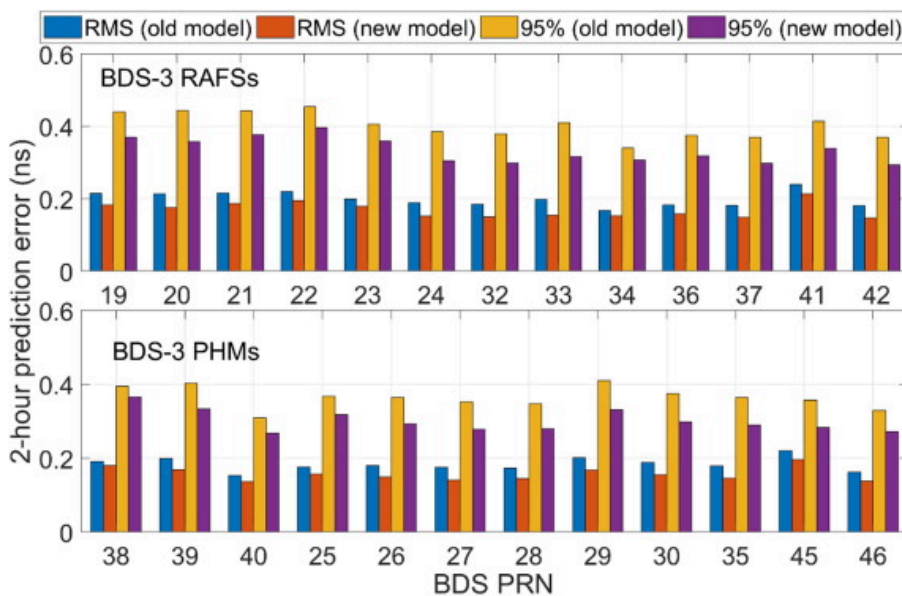
Fig. 8. Frequency stability of intersatellite clock offsets under different relativistic corrections.. Blue and red curves are the clock offsets respectively corrected by GNSS conventional relativistic correction and high-accuracy relativistic correction.

Top left panel of Fig. 8 plots the frequency stability of intersatellite clock offsets between two IGSO satellites (C39-C40). There are two obvious “bumps” at about intervals of $4/N$ (orbital periodicity) and 7 days in the intersatellite clock offsets corrected by the GNSS conventional relativistic correction model; however, after adopting the high-accuracy relativistic correction model, these “bumps” disappear. The top middle panel of Fig. 8 plots the frequency stability of intersatellite clock offsets between MEO and IGSO satellites (C39-C27). A continuous “bump” is similarly observed within the interval from 6000s to 100000s in the intersatellite clock offsets corrected by the GNSS conventional relativistic correction model; likewise, after adopting the high-accuracy relativistic correction model, the “bumps” disappear. The top right and bottom left panels of Fig. 8 plot the frequency stability of intersatellite clock offsets between two MEO satellites on the same orbital plane and on different orbital planes, respectively, revealing obvious “bumps” at the orbital periodic interval of $4/N$. Once more, after adopting the high-accuracy relativistic correction model, the “bumps” disappear, and the Hadamard deviation becomes smoother. However, different from other panels of Fig. 8, after applying the high-accuracy relativistic correction model, while the “bumps” mostly disappear in bottom middle panel of Fig. 8, some smaller “bumps” remain. The reason for these smaller “bumps” (whose period is approximately 1 orbital period) is unknown, but only under the high-accuracy relativistic frame can their mechanism be further researched. The bottom right panel of Fig. 8 plots the frequency stability of the intersatellite clock offsets between the RAFSs and PHMs. After deducting the GNSS relativistic correction errors, the frequency instability is greatly decreased within the interval from a few thousand seconds to 100000s. These phenomena indicate the effects of GNSS relativistic correction errors not only on the clock offsets between PHMs but also on the clock offsets between RAFSs.

These analyses in the frequency domain suggest that GNSS conventional relativistic correction errors also seriously affect the frequency stability of intersatellite clock offsets. After adopting the proposed high-accuracy relativistic

correction model, the performance evaluation of both PHMs and RAFSs can be improved. Moreover, under the high-accuracy relativistic framework, smaller measurement errors that otherwise remain hidden beneath GNSS conventional relativistic errors can be detected (Delva et al. 2015). These findings further strengthen the necessity of applying a high-accuracy relativity model in time synchronization endeavors and in the evaluation of high-performance onboard atomic clocks.

Histograms visualizing the statistical results of the 2h predicted errors of the intersatellite clock offsets under different relativistic corrections are given in Fig. 9, where the blue bars are the RMS 2h predicted errors under the GNSS conventional relativistic correction model, the orange bars are the 95% predicted errors under the GNSS conventional relativistic correction model, the red bars are the RMS 2h predicted errors under the high-accuracy relativistic correction model, and the purple bars are the 95% errors under the high-accuracy relativistic correction model. The top panel shows the predicted errors between RAFSs. Under the GNSS conventional relativistic correction model, the average RMS predicted error of the intersatellite clock offsets is approximately 0.199ns, and the average 95% error is 0.403ns. Under the high-accuracy relativistic correction model, the average RMS and average 95% 2h predicted errors can decrease by approximately 15.1% and 17.1%, respectively, to 0.169ns and 0.334ns. Likewise, the bottom panel shows the predicted errors between PHMs. Under the GNSS conventional relativistic correction model, the average RMS predicted error of the intersatellite clock offsets is approximately 0.183ns, and the average 95% error is 0.365ns. Under the high-accuracy relativistic correction model, the 2h predicted errors can be reduced by approximately 14.6% and 17.5%, respectively, to 0.156ns and 0.301ns. The above results indicate that if the proposed high-accuracy relativistic correction model is adopted to replace the GNSS conventional relativistic correction model, the accuracy of clock offsets can be effectively improved, which will facilitate a reduction in the signal-in-space ranging error (SISRE).



[Download : Download high-res image \(342KB\)](#)

[Download : Download full-size image](#)

Fig. 9. Two-hour predicted errors of intersatellite clock offsets under different relativistic corrections. The blue and orange bars are the results corrected by GNSS conventional relativistic correction. The red and purple bars are the results corrected by high-accuracy relativistic correction.

5. Conclusion and outlook

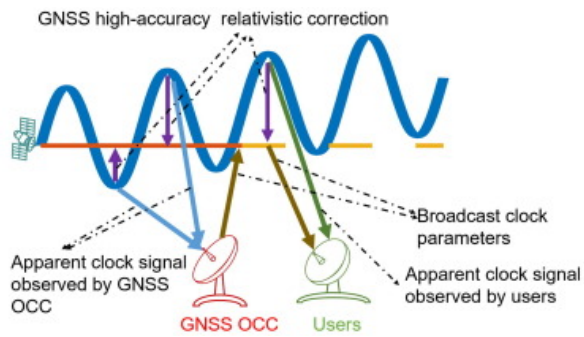
We presented a high-accuracy relativistic correction method for GNSS time synchronization based on the relationship between the satellite proper and coordinate times. Furthermore, based on this high-accuracy relativistic correction

method, we analyze the characteristics of GNSS conventional relativistic correction errors. The results of various analyses show the following:

- 1) GNSS conventional relativistic correction errors in BDS-3 satellites mainly include long-term errors, a half-year periodic term (about 183 days), a half-month periodic term (about 14 days), and a half-orbit periodic term (about 6 h for MEO satellites and about 12 h for IGSO satellites).
- 2) For IGSO platforms, the long-term and long periodic terms are obvious, and the frequency drift can reach $2.0E-21 s/s^2$. The amplitude of the half-month periodic term can reach 0.4 ns, and the amplitude of the half-orbit periodic term can reach 0.08 ns. For MEO platforms, the amplitude of the half-year periodic term can reach 1.4 ns, the amplitude of the half-month periodic term can reach 0.3 ns, and the amplitude of the half-orbit periodic term can reach 0.07 ns.
- 3) The frequency stability of the GNSS conventional relativistic correction error is approximately $1.33E-14$ (about 10000 s) and $1.78E-15$ (about 1 day).
- 4) GNSS conventional relativistic correction errors will deteriorate the prediction ability of onboard atomic clocks. The 95% uncertainty in the predicted GNSS conventional relativistic correction error can reach 0.25 ns for MEO satellites and 0.31 ns for IGSO satellites within 1 day.

Then, corrected by GNSS relativistic conventional correction, some obvious periodic terms are still found in the BDS-3 high-accuracy intersatellite clock offsets. The periodic terms are mainly caused by the more exact relativistic effects. After adopting the high-accuracy relativistic correction model, the frequency instability obviously decreases, the 30-day fitting residual of intersatellite clock offsets can decrease from 0.39 ns to 0.28 ns (about 28%), and the 24-day fitting residual of intersatellite clock offsets can decrease from 0.12 ns to 0.05 ns (about 60%). Further analyses demonstrate that the average 2 h 95% predicted errors of intersatellite clock offsets can decrease by approximately 17% from 0.38 ns to 0.32 ns. These results, on the one hand, indicate that both PHMs and ISL observation of BDS-3 were so stable, clearly detecting sub-daily errors of the conventional relativity correction, and in some cases, even sub-monthly ones, on the other hand, indicate that the clock offsets products corrected by GNSS conventional relativistic correction model is not sufficient to support BDS-3 onboard atomic clocks and time synchronization research at present. In contrast, adopting the high-accuracy relativistic correction model is expected to facilitate improvements in the accuracy of both time synchronization and clock offset predictions.

In the future, to improve their serviceability, both the satellites and the ground stations in GNSSs will be equipped with higher-performance atomic clocks and higher-precision measurement equipment (Glaser et al. 2020). Moreover, low Earth orbit (LEO) constellations, which suffer more serious relativistic effects (Larson et al., 2007, LeMaster, 2021), will be introduced to enhance the serviceability of GNSSs (Li et al., 2019, Zeng et al., 2019). Both of them require the support of a highly accurate relativistic framework. Therefore, if high-accuracy clock offset through prediction is a target, both GNSS OCCs and users are advised to employ higher-accuracy relativistic correction models to correct apparent clock offsets in the future. A feasible approach is visualized in Fig. 10. First, GNSSs could use (9) to correct apparent clock offsets (blue lines) to obtain the parameters of the clock offsets described in proper time (red line), which is used to make predictions and broadcasts to users (yellow lines). On the other hand, according to the broadcast ephemeris, users could use (9) to correct the parameters of the clock offsets to obtain the predicted apparent clock offsets or make the opposite correction in the measurements.



[Download : Download high-res image \(188KB\)](#)

[Download : Download full-size image](#)

Fig. 10. GNSS clock parameter generation and application under the proposed high-accuracy relativistic correction model.

Finally, this paper only derives a numerical expression of the relativistic correction model and does not offer an analytic solution that includes all kinds of perturbations. Previous works have already developed and discussed relativistic analytic solution (Colmenero et al., 2021, Kouba, 2004, Ashby, 2003). But due to frequent orbital maneuvers and long-term variation of orbit elements of BDS-3 satellite, which one of them is suitable for BDS-3 needs to be further compared and discussed. Therefore, the work presented in this paper is just the beginning, and further work is warranted.

Declaration of Competing Interest

The authors declare that they have no known competing financial interests or personal relationships that could have appeared to influence the work reported in this paper.

Acknowledgment

This work was supported by the National Natural Science Foundation of China (Grant Nos. 12173072). And the authors wish to thank the editor and the reviewers, whose valuable comments and suggestions helped improve this paper enormously.

[Recommended articles](#)

References

[Ashby, 2003](#) N. Ashby

(2003) "Relativity in the Global Positioning System"

Living Rev. Relativ., 6 (2003), p. 1, [10.12942/lrr-2003-1](https://doi.org/10.12942/lrr-2003-1) ↗

[View in Scopus](#) ↗ [Google Scholar](#) ↗

[BaoJun et al., 2021](#) L.I.N. BaoJun, L.I. ShaoQiang, R. Dong, L.I.U. YinChun, W. Gong

On-orbit evaluation of influence of magnetic-induced frequency shift on space borne atomic clock

Sci. Sin. Phys. Mech. Astron., 51 (2021), Article 019514, [10.1360/SSPMA-2020-0225](https://doi.org/10.1360/SSPMA-2020-0225) ↗

[Google Scholar](#) ↗

[Cacciapuoti and Salomon, 2011](#) L. Cacciapuoti, C. Salomon

Atomic clock ensemble in space

J. Phys. Conf. Ser., 327 (2011), p. 012049, [10.1088/1742-6596/327/1/012049](https://doi.org/10.1088/1742-6596/327/1/012049) ↗

[View in Scopus](#) ↗ [Google Scholar](#) ↗

Carson and Haljasmaa, 2015 C.G. Carson, I.V. Haljasmaa

Proper calculation of a modulation half cycle from the Allan deviation

Metrologia: Int. J. Sci. Metrol.: = Internationale Zeitschrift für Wissenschaftliche Metrologie, 52 (6) (2015), pp. L31-L33, [10.1088/0026-1394/52/6/L31](https://doi.org/10.1088/0026-1394/52/6/L31) ↗

[View in Scopus](#) ↗ [Google Scholar](#) ↗

Chen et al., 2020 J.P. Chen, X.G. Hu, C.P. Tang, S.S. Zhou, Y.F. Yang, J.Y. Pan, H. Ren, Y.X. Ma, Q.N. Tian, B. Wu, Y. Yu

SIS accuracy and service performance of the BDS-3 basic system

Sci. China-Phys. Mech. Astron., 63 (2020), Article 269511, [10.1007/s11433-019-1468-9](https://doi.org/10.1007/s11433-019-1468-9) ↗

[View in Scopus](#) ↗ [Google Scholar](#) ↗

Colmenero et al., 2021 N.P. Colmenero, J.V.A. Córdoba, M.J. Fullanaifonso

Relativistic positioning: including the influence of the gravitational action of the sun and the moon and the Earth's oblateness on Galileo satellites

Astrophys. Space Sci., 366 (7) (2021), pp. 1-19, [10.1007/s10509-021-03973-z](https://doi.org/10.1007/s10509-021-03973-z) ↗

[Google Scholar](#) ↗

Delva et al., 2018 P. Delva, S. Bertone, et al.

Gravitational redshift test using eccentric galileo satellites

Phys. Rev. Lett., 121 (23) (2018), [10.1103/PhysRevLett.121.231101](https://doi.org/10.1103/PhysRevLett.121.231101) ↗
id.231101

[Google Scholar](#) ↗

Delva et al., 2015 P. Delva, A. Hees, S. Bertone, et al.

Test of the gravitational redshift with stable clocks in eccentric orbits: application to Galileo satellites 5 and 6 Class

Quantum Grav., 32 (2015), p. 232003, [10.1088/0264-9381/32/23/232003](https://doi.org/10.1088/0264-9381/32/23/232003) ↗

[View in Scopus](#) ↗ [Google Scholar](#) ↗

Folkner et al., 2008 Folkner, W.M., Williams, J.G., Boggs, D.H., 2008. The Planetary and Lunar Ephemeris DE 421, IPN

Progress Report 42-178, August 15, 2009, 31 pp., see http://ipnpr.jpl.nasa.gov/progress_report/42-178/178C.pdf ↗.

[Google Scholar](#) ↗

Deng et al., 2022 Zhi. Deng, J. Wang, M. Ge

The GBM rapid product and the improvement from undifferenced ambiguity resolution

Acta Geodaetica et Cartographica Sinica, 51 (4) (2022), pp. 544-555, [10.11947/j.AGCS.2022.20220022](https://doi.org/10.11947/j.AGCS.2022.20220022) ↗

[View in Scopus](#) ↗ [Google Scholar](#) ↗

Formichella et al., 2021 V. Formichella, L. Galleani, G. Signorile, et al.

Time-frequency analysis of the Galileo satellite clocks: looking for the J2 relativistic effect and other periodic variations

GPS Solut., 25 (2021), p. 56, [10.1007/s10291-021-01094-2](https://doi.org/10.1007/s10291-021-01094-2) ↗

[View in Scopus](#) ↗ [Google Scholar](#) ↗

Giorgi et al., 2019 G. Giorgi, T. Schmidt, et al.

Advanced technologies for satellite navigation and geodesy

Adv. Space Res., 64 (2019), pp. 1256-1273, [10.1016/j.asr.2019.06.010](https://doi.org/10.1016/j.asr.2019.06.010) ↗

 [View PDF](#) [View article](#) [View in Scopus](#) ↗ [Google Scholar](#) ↗

[Glaser et al., 2020](#) S. Glaser, G. Michalak, B. Männel, R. König, K.H. Neumayer, H. Schuh

Reference system origin and scale realization within the future GNSS constellation “Kepler”

J. Geod., 94 (2020), p. 117, [10.1007/s00190-020-01441-0](https://doi.org/10.1007/s00190-020-01441-0) ↗

[View in Scopus](#) ↗ [Google Scholar](#) ↗

[Han and Cai, 2019](#) C. Han, Z. Cai

Relativistic effects to the onboard BeiDou satellite clocks

Navigation, 66 (2019), pp. 49-53, [10.1002/navi.294](https://doi.org/10.1002/navi.294) ↗

[View in Scopus](#) ↗ [Google Scholar](#) ↗

[Han et al., 2021](#) C. Han, L. Liu, Z. Cai, Y. Lin

The space–time references of BeiDou navigation satellite system

Satell. Navig., 2 (2021), p. 18, [10.1186/s43020-021-00044-0](https://doi.org/10.1186/s43020-021-00044-0) ↗

[Google Scholar](#) ↗

[Hermann, et al., 2018](#) S. Hermann, *et al.*

Test of the gravitational redshift with galileo satellites in an eccentric orbit

Phys. Rev. Lett., 121 (23) (2018), [10.1103/PhysRevLett.121.231102](https://doi.org/10.1103/PhysRevLett.121.231102) ↗
id.231102

[Google Scholar](#) ↗

[Johnston et al., 2017](#) G. Johnston, A. Riddell, G. Hausler

The international GNSS service

P.J. Teunissen, O. Montenbruck (Eds.), Springer handbook of global navigation satellite systems, Springer, Cham (2017), pp. 967-982, [10.1007/978-3-319-42928-1_33](https://doi.org/10.1007/978-3-319-42928-1_33) ↗

[View in Scopus](#) ↗ [Google Scholar](#) ↗

[Kopeikin et al., 2011](#) S. Kopeikin, M. Efroimsky, G. Kaplan

(2011) Relativistic celestial mechanics of the solar system

Wiley, Berlin (2011)

[Google Scholar](#) ↗

[Kouba, 2002](#) J. Kouba

Relativistic time transformations in GPS

GPS Solut., 5 (2002), pp. 1-9, [10.1007/pl00012907](https://doi.org/10.1007/pl00012907) ↗

[Google Scholar](#) ↗

[Kouba, 2004](#) J. Kouba

Improved relativistic transformations in GPS

GPS Solut., 8 (2004), pp. 170-180, [10.1007/s10291-004-0102-x](https://doi.org/10.1007/s10291-004-0102-x) ↗

[View in Scopus](#) ↗ [Google Scholar](#) ↗

[Kouba, 2019](#) J. Kouba

Relativity effects of Galileo passive hydrogen maser satellite clocks

GPS Solut., 23 (2019), [10.1007/s10291-019-0910-7](https://doi.org/10.1007/s10291-019-0910-7) ↗

[Google Scholar](#) ↗

[Kouba, 2021](#) J. Kouba

Testing of general relativity with two Galileo satellites in eccentric orbits

GPS Solut., 25 (2021), p. 139, [10.1007/s10291-021-01174-3](https://doi.org/10.1007/s10291-021-01174-3) ↗

[View in Scopus](#) ↗ [Google Scholar](#) ↗

[Kozai, 1959](#) Y. Kozai

The motion of a close Earth satellite

Astron. J., 64 (1959), pp. 367-377, [10.1086/107957](https://doi.org/10.1086/107957) ↗

[Google Scholar](#) ↗

[Larson et al., 2007](#) K.M. Larson, N. Ashby, C. Hackman, *et al.*

(2007) An assessment of relativistic effects for low Earth orbiters: the GRACE satellites

Metrologia, 44 (6) (2007), pp. 484-490, [10.1088/0026-1394/44/6/007](https://doi.org/10.1088/0026-1394/44/6/007) ↗

[View in Scopus](#) ↗ [Google Scholar](#) ↗

[LeMaster, 2021](#) LeMaster, Edward A., 2021. A comparison of relativistic impacts on satellite timekeeping for various orbits. In: Proceedings of the 52nd Annual Precise Time and Time Interval Systems and Applications Meeting, January 2021, pp. 326-337. <https://doi.org/10.33012/2021.17769> ↗.

[Google Scholar](#) ↗

[Li et al., 2019](#) X.X. Li, Y.Q. Yuan, J. Huang, Y. Zhu, J. Wu, Y. Xiong, X. Li, K. Zhang

Galileo and QZSS precise orbit and clock determination using new satellite metadata

J. Geod., 93 (2019), pp. 1123-1136, [10.1007/s00190-019-01230-4](https://doi.org/10.1007/s00190-019-01230-4) ↗

[Google Scholar](#) ↗

[Liu, 1977a](#) L. Liu

A calculating method of perturbation of artificial satellite

Chin. Astron., 1 (1977), pp. 63-78, [10.1016/0146-6364\(77\)90023-8](https://doi.org/10.1016/0146-6364(77)90023-8) ↗

[Google Scholar](#) ↗

[Liu, 1977b](#) L. Liu

A solution of the motion of an artificial satellite in the vicinity of the critical inclination

Chin. Astron., 1 (1977), pp. 31-42, [10.1016/0146-6364\(77\)90020-2](https://doi.org/10.1016/0146-6364(77)90020-2) ↗

[Google Scholar](#) ↗

[Mei et al., 2021](#) G.H. Mei, F. Zhao, F. Qi, *et al.*

Characteristics of the space-borne rubidium atomic clocks for the BeiDou III navigation satellite system

Sci. Sin-Phys. Mech. Astron., 51 (2021), Article 019512, [10.1360/SSPMA-2020-0245](https://doi.org/10.1360/SSPMA-2020-0245) ↗

[Google Scholar](#) ↗

[Montenbruck et al., 2020](#) Montenbruck, O., Steigenberger, P., Hauschild, A., 2020. Comparing the 'Big 4' - a user's view on GNSS performance. In: 2020 IEEE/ION Position, Location and Navigation Symposium (PLANS). IEEE, Portland, OR, USA, pp 407-418

[Google Scholar](#) ↗

[Montenbruck et al., 2015](#) O. Montenbruck, P. Steigenberger, U. Hugentobler

Enhanced solar radiation pressure modeling for Galileo satellites

J. Geod., 89 (2015), pp. 283-297, [10.1007/s00190-014-0774-0](https://doi.org/10.1007/s00190-014-0774-0) ↗

[View in Scopus](#) [Google Scholar](#)

[Montenbruck et al., 2017](#) O. Montenbruck, P. Steigenberger, L. Prange, *et al.*

The multi-GNSS experiment (MGEX) of the international GNSS Service (IGS) – achievements, prospects and challenges

Adv. Space Res., 59 (2017), pp. 1671-1697, [10.1016/j.asr.2017.01.011](#)

 [View PDF](#) [View article](#) [View in Scopus](#) [Google Scholar](#)

[Pan et al., 2018](#) J. Pan, X. Hu, S. Zhou, C. Tang, R. Guo, L. Zhu, G. Tang, G. Hu

Time synchronization of new-generation BDS satellites using inter-satellite link measurements

Adv. Space Res., 61 (2018), pp. 145-153, [10.1016/j.asr.2017.10.004](#)

 [View PDF](#) [View article](#) [View in Scopus](#) [Google Scholar](#)

[Petit and Luzum, 2010](#) Petit and Luzum IERS conventions, 2010. In: Petit, G., Luzum, B. (Eds.) IERS technical note 36.

Verlag des Bundesamts für Kartographie und Geodäsie, Frankfurt am Main, p 179. <http://www.iers.org/TN36/>

[Google Scholar](#)

[Proia et al., 2014](#) Proia, A., Bourgolet, F., d'Heeger, A., *et al.*, 2014. Performance results of the Galileo precise timing

facility. In: 2014 European frequency and time forum (EFTF). IEEE, Neuchatel, Switzerland, pp 463-467. doi:

10.1109/EFTF.2014.7331536.

[Google Scholar](#)

[Senior and Coleman, 2017](#) K.L. Senior, M.J. Coleman

The next generation GPS time

Navigation, 64 (2017), pp. 411-426, [10.1002/navi.208](#)

[Google Scholar](#)

[Shuai et al., 2021](#) T. Shuai, B.J. Lin, J. Zhang, *et al.*

Performances and telemetres analysis of BD satellite passive hydrogen maser

Sci. Sin-Phys. Mech. Astron., 51 (2021), Article 019513, [10.1360/SSPMA-2020-0226](#)

[Google Scholar](#)

[Soffel and Han, 2019](#) M. Soffel, W.-B. Han

Applied General Relativity: Theory and Applications in Astronomy, Celestial Mechanics and Metrology

Springer, Berlin (2019)

10.1007/978-3-030-19673-8

[Google Scholar](#)

[Soffel et al., 2003](#) M. Soffel, S. Klioner, G. Petit, *et al.*

The IAU 2000 resolutions for astrometry, celestial mechanics, and metrology in the relativistic framework: explanatory supplement

Astron. J., 126 (2003), pp. 2687-2706, [10.1086/378162](#)

[View in Scopus](#) [Google Scholar](#)

[Steigenberger and Montenbruck, 2016](#) P. Steigenberger, O. Montenbruck

Galileo status: orbits, clocks, and positioning

GPS Solut., 21 (2016), pp. 319-331, [10.1007/s10291-016-0566-5](#)

[Google Scholar](#)

[Tang et al., 2016](#) C. Tang, X. Hu, S. Zhou, *et al.*

Improvement of orbit determination accuracy for Beidou navigation satellite system with two-way satellite time frequency transfer

Adv. Space Res., 58 (2016), pp. 1390-1400, [10.1016/j.asr.2016.06.007](#) ↗

 [View PDF](#) [View article](#) [View in Scopus](#) ↗ [Google Scholar](#) ↗

[Tang et al., 2018](#) C. Tang, X. Hu, S. Zhou, L. Liu, J. Pan, L. Chen, R. Guo, L. Zhu, G. Hu, X. Li, F. He, Z. Chang

Initial results of centralized autonomous orbit determination of the new-generation BDS satellites with inter-satellite link measurements

J. Geod., 92 (2018), pp. 1155-1169, [10.1007/s00190-018-1113-7](#) ↗

[View in Scopus](#) ↗ [Google Scholar](#) ↗

[Wang et al., 2017](#) Y.P. Wang, Z.P. Lv, L.Y. Li, S.F. Zhai

Analysis of the long-term performance of GPS BLOCK IIF satellite atomic clocks

Acta Astron Sin, 58 (2017), p. 20, [10.15940/j.cnki.0001-5245.2017.03.002](#) ↗

 [View PDF](#) [View article](#) [Google Scholar](#) ↗

[Wu et al., 2018](#) Z. Wu, S. Zhou, X. Hu, L. Liu, T. Shuai, Y. Xie, C. Tang, J. Pan, L. Zhu, Z. Chang

Performance of the BDS3 experimental satellite passive hydrogen maser

GPS Solut., 22 (2018), p. 44, [10.1007/s10291-018-0706-1](#) ↗

[Google Scholar](#) ↗

[Yang et al., 2021a](#) J.H. Yang, Y.Z. Song, Z.Q. Chang, X.G. Hu, S.S. Zhou, C.P. Tang

Analysis of signal-in-space ranging error of GNSS navigation message

Sci. Sin Phys. Mech. Astron., 51 (2021), Article 019508, [10.1360/sspma-2020-0227](#) ↗

[Google Scholar](#) ↗

[Yang et al., 2022](#) J. Yang, C. Tang, S. Zhou, Y. Song, J. Liu, Y. Xiang, Y. Liu, Q. Tian, Y. Yang, Z. Yang, *et al.*

High-Accuracy Clock Offsets Estimation Strategy of BDS-3 Using Multi-Source Observations

Remote Sens., 14 (2022), p. 4674, [10.3390/rs14184674](#) ↗

[View in Scopus](#) ↗ [Google Scholar](#) ↗

[Yang et al., 2019](#) Y. Yang, Y. Yang, X. Hu, J. Chen, R. Guo, C. Tang, S. Zhou, L. Zhao, J. Xu

Inter-satellite link enhanced orbit determination for BeiDou-3

J. Navig., 73 (2019), pp. 115-130, [10.1017/s0373463319000523](#) ↗

[Google Scholar](#) ↗

[Yang et al., 2021b](#) Y. Yang, Y. Yang, X. Hu, C. Tang, R. Guo, Z. Zhou, J. Xu, J. Pan, M. Su

BeiDou-3 broadcast clock estimation by integration of observations of regional tracking stations and inter-satellite links

GPS Solut., 25 (2021), pp. 1-12, [10.1007/s10291-020-01067-x](#) ↗

[Google Scholar](#) ↗

[Zeng et al., 2019](#) T. Zeng, L. Sui, X. Jia, Z. Lv, G. Ji, Q. Dai, Q. Zhang

Validation of enhanced orbit determination for GPS satellites with LEO GPS data considering multi ground station networks

Adv. Space Res., 63 (2019), pp. 2938-2951, [10.1016/j.asr.2018.06.012](#) ↗

 [View PDF](#) [View article](#) [View in Scopus](#) ↗ [Google Scholar](#) ↗

Zhang et al., 2014 K. Zhang, S. Xue, M.B. Lü

Relativistic time transfer and synchronization in the vicinity of the Earth

J. Electron. Inf. Technol., 36 (2014), pp. 1992-1998, [10.3724/SP.J.1146.2014.00107](https://doi.org/10.3724/SP.J.1146.2014.00107) ↗

[View in Scopus](#) ↗ [Google Scholar](#) ↗

Zhou et al., 2020 Zhou, W., Ruan, R., Jia, X., Jin, R., 2020. BDS-3 onboard atomic clock performance evaluation. In: China satellite navigation conference (CSNC) 2020 proceedings: volume III. Springer, Singapore, pp 134-143.

https://doi.org/10.1007/978-981-15-3715-8_13 ↗.

[Google Scholar](#) ↗

Zhou et al., 2016 S.S. Zhou, X.G. Hu, L. Liu, R. Guo, L.F. Zhu, Z.Q. Chang, C.P. Tang, X.Q. Gong, R. Li, Y. Yu

Applications of two-way satellite time and frequency transfer in the BeiDou navigation satellite system

Sci. China Phys. Mech. Astron., 59 (2016), Article 109511, [10.1007/s11433-016-0185-6](https://doi.org/10.1007/s11433-016-0185-6) ↗

[View in Scopus](#) ↗ [Google Scholar](#) ↗

Cited by (0)

© 2023 COSPAR. Published by Elsevier B.V.



All content on this site: Copyright © 2024 Elsevier B.V., its licensors, and contributors. All rights are reserved, including those for text and data mining, AI training, and similar technologies. For all open access content, the Creative Commons licensing terms apply.

